BILINGUAL PUBLISHING GROUP

Journal of Environmental & Earth Sciences

https://journals.bilpubgroup.com/index.php/jees

ARTICLE

Applicability Evaluation of Himawari-9 Downward Surface Shortwave Radiation (DSSR) Product under Complex Weather Conditions: A Case Study of Guangxi

Yiming Qin [1], Jiaqiu Hu [1], Lu Zhang [2*], Kui Huang [1], Houjian Zhan [1], Jian Tang [1]

[1] *Power Dispatching Control Center of Guangxi Power Grid, Nanning 530012, China*

[2] *National Satellite Meteorological Center, China Meteorological Administration, Beijing 100081, China*

ABSTRACT

The Advanced Himawari Imager (AHI) aboard Himawari-8/9 can provide downward surface shortwave radiation (DSSR) with 5 km and a high temporal resolution of 10 min. To evaluate its applicability under complex meteorological and topographic conditions, this study systematically assesses the overall quality of the Himawari-9 DSSR product in Guangxi region and its performance under different cloud and aerosol conditions, based on ground-observed observations from photovoltaic and meteorological stations in 2023. The overall comparison of hourly AHI DSSR and ground DSSR shows a high correlation coefficient (R = 0.85); however, there is also a large bias (RPE (relative prediction error) = 46.71%, RMSE (root mean square error) = 162.99 W/m^2). Errors are larger in spring and summer, and spatially, errors are significantly higher in the hilly and mountainous areas of northwestern Guangxi compared to the flatter southern and central regions. Satellite retrieval accuracy degrades markedly as cloud cover and aerosol level intensify, with the correlation coefficients dipping from 0.90 (clear sky) to the lowest values of 0.11 (COD (cloud optical depth) > 50) and slightly decreasing from 0.84 (0 ≤ AOD (aerosol optical depth) ≤ 0.1) to 0.79 (AOD >2), respectively. These findings reveal critical limitations of satellite DSSR products under specific atmospheric conditions, providing essential guidance for photovoltaic resource

*CORRESPONDING AUTHOR:

Lu Zhang, National Satellite Meteorological Center, China Meteorological Administration, Beijing 100081, China; Email: zl72@cma.gov.cn

ARTICLE INFO

Received: 15 January 2026 | Revised: 7 March 2026 | Accepted: 10 March 2026 | Published Online: 9 April 2026
DOI: https://doi.org/10.30564/jees.v8i4.13029

CITATION

Qin, Y., Hu, J., Zhang, L., et al., 2026. Applicability Evaluation of Himawari-9 Downward Surface Shortwave Radiation (DSSR) Product under Complex Weather Conditions: A Case Study of Guangxi. Journal of Environmental & Earth Sciences. 8(4): 102–116.
DOI: https://doi.org/10.30564/jees.v8i4.13029

assessment and power forecasting applications in Guangxi. It also serves as an important reference for the evaluation and application of satellite-derived surface radiation products at the national scale.

Keywords: Downward Surface Shortwave Radiation (DSSR); Himawari-9; Photovoltaic Stations; Cloud Optical Depth (COD); Aerosol Optical Depth (AOD)

1. Introduction

Downward surface shortwave radiation (DSSR) is a major component of the surface radiation budget[1] and plays a critical role in regulating vegetation photosynthesis, surface energy balance, and the evolution of the climate system. Consequently, the precise estimation of DSSR is of great importance for climate modeling, environmental monitoring, agricultural production, and renewable energy development[2–4]. In recent years, driven by the global transition of energy structures and the rapidly increasing demand for renewable energy, the photovoltaic (PV) industry has entered a period of rapid growth. The power generation efficiency of PV systems is highly dependent on the intensity and spatiotemporal distribution of incoming solar radiation. Consequently, obtaining high-resolution and accurate DSSR information has become a key prerequisite for optimizing PV plant site selection, system design, and operational management[5,6]. This growing demand places increasingly stringent requirements on the observation and evaluation of surface solar radiation.

Currently, surface solar radiation data are primarily derived from two sources: ground-based measurements and satellite remote sensing retrievals[7,8]. Although ground observations provide high temporal resolution and accuracy[9], their application is severely constrained by the limited number and uneven spatial distribution of stations, particularly in regions with complex terrain or remote areas, where representativeness is often insufficient[10]. In contrast, satellite remote sensing offers continuous, large-scale, and long-term radiation products, providing indispensable data support for regions lacking in situ observations[11]. Among these, the new-generation geostationary meteorological satellites Himawari-8/9, operated by the Japan Meteorological Agency, have demonstrated great potential for solar energy resource assessment owing to their high temporal resolution (up to 2.5 min) and extensive spatial coverage[12–15]. Previous studies have shown that DSSR products retrieved from Himawari-8/9 generally exhibit high accuracy and strong consistency with ground observations ($R^2 \approx 0.89$)[16–18] and outperform reanalysis products such as CERES-SYN, MERRA-2, and ERA-Interim, as well as MODIS radiation products[16,18]. However, systematic overestimation remains a common issue, particularly under conditions of heavy cloud cover or high aerosol loading[16,18,19]. Clouds and aerosols can substantially alter solar radiation transmission through scattering and absorption, while uncertainties in the parameterization of cloud and aerosol properties in current satellite retrieval algorithms continue to introduce errors in surface radiation estimates[15,20]. Although some studies have attempted to improve product accuracy by refining cloud masking techniques or incorporating more accurate atmospheric parameters, existing validation studies have primarily focused on Japan or northern China[9,19,21]. It leaves a notable research gap in humid subtropical regions with complex terrain such as Guangxi Zhuang Autonomous Region in southern China—where cloud cover is persistent, aerosol variability is high, and conventional observation networks are sparse. This study addresses that gap by conducting the first comprehensive regional evaluation of the Himawari-9 DSSR product over Guangxi.

Guangxi is located in the subtropical monsoon climate zone, with annual total solar radiation reaching approximately 5,000 MJ/m^2[22], yet its solar energy resources remain significantly underexploited relative to their potential. Geographically, Guangxi is geographically dominated by complex hilly and mountainous terrain, characterized by persistent humidity, frequent cloud cover, and abundant precipitation. In addition, aerosol concentrations are influenced by both monsoonal transport and local emissions, resulting in pronounced spatiotemporal variability in surface solar radiation[23]. Meanwhile, local energy consumption still relies heavily on fossil fuels such as coal and petroleum, highlighting an urgent need to promote large-scale development of renewable energy, particularly photovoltaic power, to optimize the energy structure and facilitate a green and low-carbon transition[22]. Nevertheless, Guangxi currently

has only three national benchmark radiation stations operated by the China Meteorological Administration (CMA), which are too sparse to capture the fine-scale spatial heterogeneity of solar radiation across the region, thereby severely limiting PV resource assessment and optimal plant deployment.

The primary innovation of this study lies in the first-time utilization of measured irradiance data from 55 densely distributed PV power stations across Guangxi, constituting the most comprehensive and representative surface solar radiation observation network in the region to date. In contrast to previous studies that relied on sparse meteorological stations, this unprecedented dataset enables precise characterization of local DSSR variability under complex terrain conditions and provides an unprecedented high-spatial-resolution reference for evaluating the regional applicability of satellite-derived products. Based on this dataset, we systematically assess the overall performance of the Himawari-9 DSSR product over Guangxi and further analyze retrieval errors under different cloud optical depth (COD) and aerosol optical depth (AOD) conditions to elucidate the influence mechanisms of clouds and aerosols. The results of this study not only provide a scientific basis for photovoltaic industry planning in Guangxi but also offer methodological support for improving solar radiation retrieval accuracy from geostationary satellites in humid and cloud-prone regions. The remainder of this paper is organized as follows: Section 2 describes the data and evaluation methods used in this study; Section 3 presents the assessment results of the Himawari-9 DSSR product under different cloud and aerosol conditions; and Section 4 summarizes the main conclusions.

2. Data and Method

2.1. Himawari-9 Products

Himawari-9 is a new-generation geostationary meteorological satellite successfully launched by the Japan Meteorological Agency (JMA) in 2016 and officially put into operational service in 2022 as the successor to Himawari-8. The satellite is equipped with the Advanced Himawari Imager (AHI), which consists of 16 spectral channels spanning the visible to infrared spectrum (0.47–13.3 μm). The spatial resolution is 0.5–1 km for visible bands and 2 km for infrared bands. AHI primarily observes the Asia–Pacific region (60° S–60° N, 80° E–160° E), providing full-disk images every 10 min, with a temporal resolution of up to 2.5 min for targeted regional observations. Himawari-9 products include Level-1 datasets at 2 km and 5 km resolution, as well as Level-2 and Level-3 products—such as aerosol, cloud, sea surface temperature, shortwave radiation, chlorophyll-a, and wildfire products—at comparable spatial resolutions.

In this study, we employ the Himawari-9 Level-2 DSSR product for the year 2023, which has a spatial resolution of 5 km and a temporal resolution of 10 min. This product is retrieved based on plane-parallel atmospheric radiative transfer theory, in which the atmosphere is simplified as a "single-layer clear atmosphere underlying a single-layer cloud." This framework enables the separation of the attenuation effects of clear-sky atmospheric constituents and clouds on incoming solar radiation. The downward surface shortwave radiation received at the surface is calculated as follows [20]

$$E = E_{clear}(1 - A)(1 - A_s)^{-1}(1 - S_a A)^{-1} \quad (1)$$

where E_{clear} denotes the surface solar radiation under clear–sky conditions, A is the cloud albedo, A_s is the surface albedo, and S_a represents the planetary albedo. Under clear-sky conditions, A is equivalent to A_s. This algorithm is computationally efficient and avoids explicit cloud screening and complex assumptions. However, it operates under the assumption of aerosol-free clear-sky conditions and does not consider cloud phase when determining cloud reflectance. As a result, systematic biases may arise under conditions of heavy aerosol loading or extensive cloud cover. Therefore, a systematic evaluation of the Himawari-9 surface solar radiation product under different cloud and aerosol scenarios is necessary.

To this end, we simultaneously employed the Himawari-9 Level-2 AOD and COD products for 2023, which have the same spatial and temporal resolutions as the DSSR product, to facilitate scenario-based error analysis. The Himawari-9 AOD product has been shown to exhibit good agreement with ground-based observations (e.g., AERONET) and reliable spatiotemporal representativeness [24]. Although comprehensive ground validation of the Himawari-9 cloud products remains limited, the AHI cloud mask has an accuracy of approximately 0.85 compared with MODIS products [25]. Moreover, COD retrieved from AHI observations shows slightly higher correlation with ground-based sky radiometer measurements than MODIS COD products [26], indicating reasonable reliability in cloud property characterization.

2.2. Photovoltaic Stations and CMA Observations

Surface solar radiation observations collected in Guangxi during 2023 from photovoltaic (PV) power stations and national benchmark climate stations operated by the CMA are used to evaluate the Himawari-9 DSSR product. All PV stations are equipped with high-precision solar radiation monitoring systems capable of simultaneously measuring global horizontal irradiance (GHI), direct normal irradiance (DNI), and diffuse horizontal irradiance (DHI), with a temporal resolution of 15 min. These observations not only support real-time operational monitoring and power generation efficiency assessment of PV plants but also provide valuable high-resolution ground truth data for regional solar radiation studies. Compared with conventional meteorological stations, PV stations are widely distributed across diverse land surfaces in Guangxi, including hills, mountains, and river valleys, encompassing complex terrain and heterogeneous climatic conditions. This substantially enhances the spatial representativeness of the observation network—an advantage that is difficult to achieve using sparse meteorological stations alone. The CMA national stations provide hourly solar radiation observations conforming to World Meteorological Organization (WMO) standards, including GHI, DNI, and DHI components, and are characterized by long-term stability and high calibration accuracy, serving as reliable regional reference benchmarks.

To construct a unified and robust evaluation dataset, all raw observations were aggregated into hourly averages and subjected to strict quality control procedures. All data were required to pass two limit tests recommended by the Baseline Surface Radiation Network (BSRN):

Physically possible limits:

$$-4\,W \bullet m^{-2} < DSSR < S_0 \times 1.5 \times \mu^{1.2} + 100\,W \bullet m^{-2} \quad (2)$$

Extremely rare limits:

$$-2\,W \bullet m^{-2} < DSSR < S_0 \times 1.2 \times \mu^{1.2} + 50\,W \bullet m^{-2} \quad (3)$$

where S_0 is the solar constant and μ is the cosine of the solar zenith angle. In addition, the following anomalous data were excluded: (1) records with identical values for three consecutive hours, indicating potential instrument malfunction; (2) data violating energy conservation relationships (e.g., GHI smaller than DNI or DHI); (3) stations with an annual quality-control pass rate below 70%; and (4) stations with fewer than 300 valid observation hours in 2023. After this multi-level quality control process, 49.5% of the original ground observations are retained. Among the excluded records, approximately 12.6% fail the BSRN limits, 8.9% are flagged for three consecutive identical values, and 25.5% violate energy conservation relationships; the remainder (about 3.5%) are excluded at the station level for insufficient annual data coverage. The final validation dataset consists of surface solar radiation measurements from 55 distributed PV stations and three CMA national benchmark stations (**Figure 1**), forming a high-quality and spatially representative reference dataset for comprehensively assessing the performance of the Himawari-9 DSSR product under the complex geographical and meteorological conditions of Guangxi.

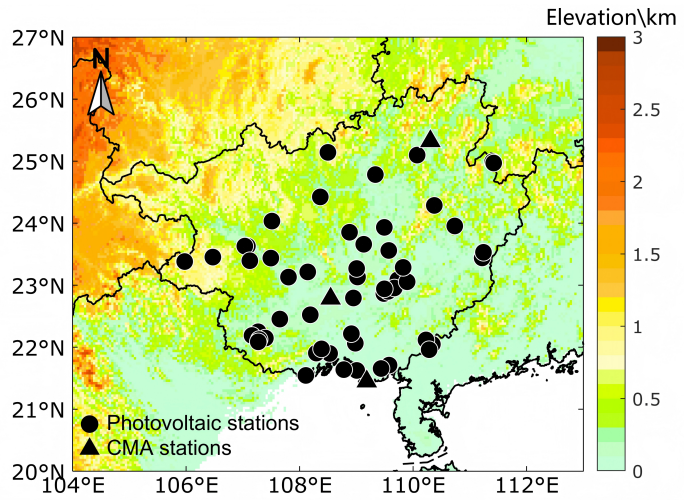

Figure 1. Distribution of ground observation stations in Guangxi.

Note: Black circles represent photovoltaic stations, and black triangles represent CMA observation stations.

2.3. Evaluation Methods

Figure 2 presents the spatial distribution of the annual mean DSSR in Guangxi for 2023, where quality-controlled ground observations are superimposed onto the corresponding Himawari-9 satellite-derived DSSR product. As shown, the Himawari-9 retrievals are generally higher than ground-based observations, indicating a systematic overestimation. For quantitative evaluation, ground-based DSSR measurements were temporally and spatially matched with the corresponding Himawari-9 DSSR, COD, and AOD products. Specifically, for each ground observation time, the satellite pixel closest in time (within ±1 h) and space (nearest 5 km grid center) was selected as the matched sample.

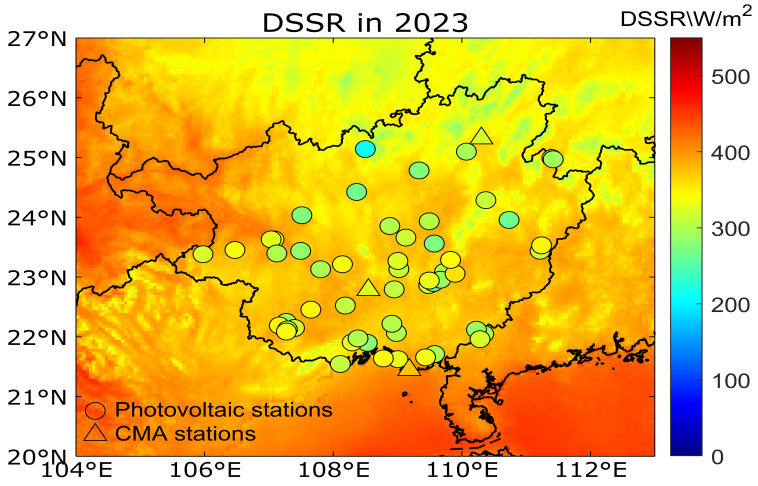

Figure 2. Annual mean DSSR in Guangxi for 2023.

Note: DSSR observations from photovoltaic stations (circles) and CMA stations (triangles) are superimposed on the Himawari-9 satellite product. Ground observation stations DSSR and Himawari-9 DSSR share the color bar on the right side.

To quantitatively assess the retrieval accuracy, four commonly used statistical metrics are employed for evaluation: the correlation coefficient (R), root mean square error (RMSE), relative prediction error (RPE), and mean bias error (MBE). These metrics are calculated as follows:

$$R = \frac{\sum_{i=1}^{N}\left(R_s^i - \overline{R_s}\right)\sum_{i=1}^{N}\left(R_g^i - \overline{R_g}\right)}{\sqrt{\sum_{i=1}^{N}\left(R_s^i - \overline{R_s}\right)^2 \sum_{i=1}^{N}\left(R_g^i - \overline{R_g}\right)^2}} \quad (4)$$

$$RMSE = \sqrt{\frac{1}{N}\sum_{i=1}^{N}\left(R_s^i - R_g^i\right)^2} \quad (5)$$

$$RPE = \frac{RMSE}{\overline{R_g}} \quad (6)$$

$$MBE = \frac{\sum_{i=1}^{N}\left(R_s^i - R_g^i\right)}{N} \quad (7)$$

where R_s denotes satellite-retrieved DSSR, R_g denotes ground-measured DSSR, N is the total number of matched samples. The correlation coefficient (R) is utilized to evaluate the linear consistency between satellite products and ground truths, while RMSE and MBE provide insights into the magnitude of random and systematic errors, respectively. Furthermore, the RPE is included as a dimensionless metric to facilitate the comparison of retrieval performance across different climatic zones and seasons, regardless of the absolute magnitude of solar irradiance. These four complementary metrics—*R* for variability capture, *MBE* for systematic bias, *RMSE* for total error, and *RPE* for relative accuracy—are calculated across seasonal, diurnal, and atmospheric scenarios to provide a multidimensional assessment.

3. Results and Analysis

3.1. Overall Evaluation of the Himawari-9 DSSR Product

Using surface solar radiation observations from photovoltaic (PV) stations and China Meteorological Administration (CMA) national reference stations in Guangxi for 2023, a quantitative evaluation of the Himawari-9 downward surface shortwave radiation (DSSR) product is conducted.

Ground observations are temporally and spatially matched with satellite pixel values, yielding the density scatterplots presented in **Figure 3**. As illustrated in **Figure 3a**, ground-based measurements and the Himawari-9 DSSR product exhibit a strong linear correlation over Guangxi, characterized by a correlation coefficient (R) of 0.85. However, the root mean square error (RMSE) reaches 162.99 W/m^2, indicating the existence of substantial systematic discrepancies between the two datasets. The majority of data pairs gravitate towards the 1:1 reference line (black dashed line in **Figure 3a**), although a number of outliers deviate markedly from the high-density region. Specifically, when DSSR is below 1,000 W/m^2, the Himawari-9 product tends to overestimate surface radiation, whereas under strong radiation conditions (DSSR > 1,000 W/m^2), a certain degree of underestimation is observed. This asymmetric bias contributes to the relatively high RMSE. In addition, the relative prediction error (RPE) reaches 46.71%, indicating a large relative deviation between satellite-derived and ground-observed mean values. The mean bias error (MBE) of 51.53 W/m^2 further confirms that the Himawari-9 product systematically overestimates DSSR over the Guangxi region.

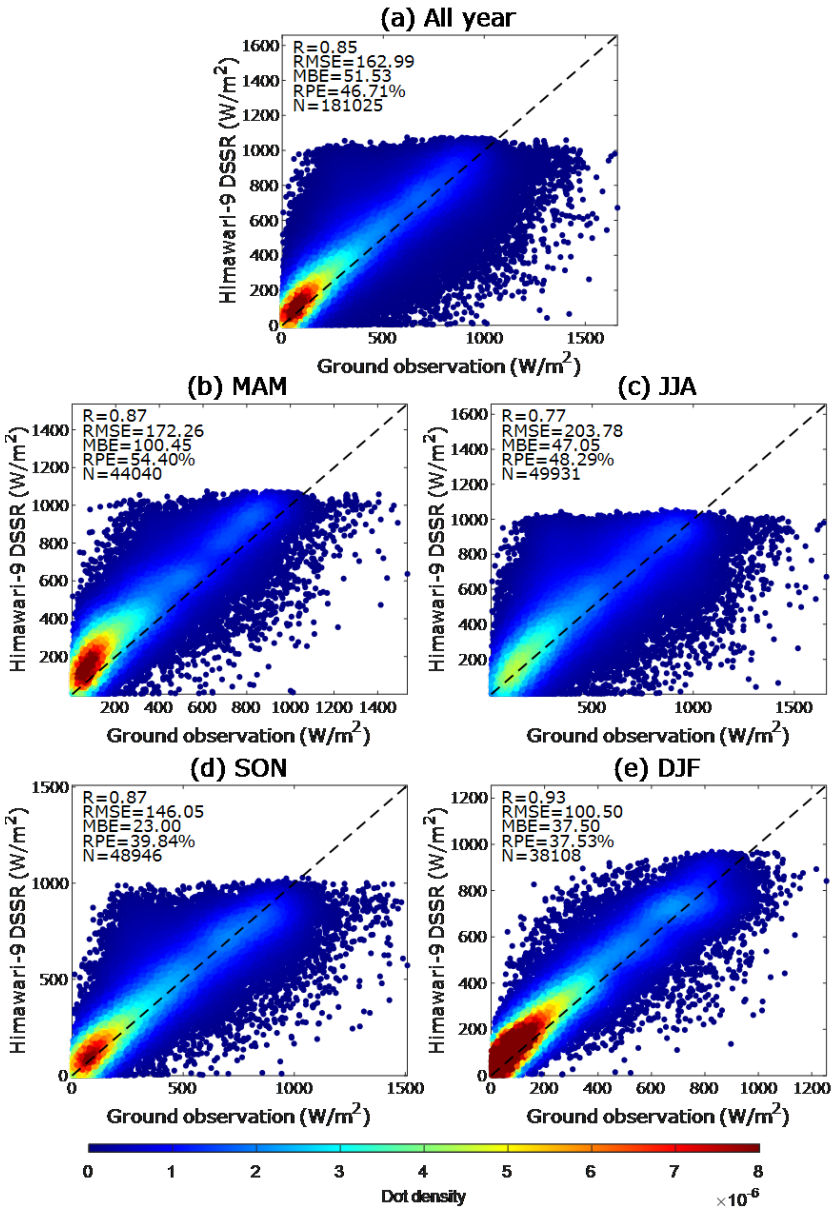

Figure 3. Scatterplots of DSSR between Himawari-9 satellite retrievals (vertical axis) and ground station observations (horizontal axis) in 2023. (**a**) Annual scatterplot; (**b**)–(**e**) scatterplots for spring (MAM), summer (JJA), autumn (SON), and winter (DJF), respectively.

Note: The black dashed line represents the 1:1 line. Point colors indicate density, with red denoting higher densities than blue.

Seasonal variations reveal that discrepancies between ground observations and the Himawari-9 DSSR product are particularly pronounced in spring (MAM) and summer (JJA) (**Figures 3** and **4**). As shown in **Figure 3c**, the correlation coefficient in summer deteriorates to 0.77, substantially lower than in other seasons, indicating reduced consistency during this period. Summer also exhibits the peak RMSE, reaching 203.78 W/m^2, being the only season exceeding 200 W/m^2. While this magnitude is partially reflective of the higher solar radiation intensity in the Northern Hemisphere summer, it also highlights larger retrieval uncertainties in the Himawari-9 product during this season. In contrast, the highest RPE (54.40%) occurs in spring, exceeding the summer value of 48.29%. Moreover, spring exhibits the largest MBE (100.45 W/m^2) among all seasons, suggesting that the Himawari-9 product is particularly prone to overestimating DSSR during spring in Guangxi. Monthly variations of the statistical metrics in 2023 (**Figure 4**) show that the minimum R and maximum RMSE occur in July. This is mainly attributed to frequent summer precipitation and the presence of thick and extensive cloud cover, which interferes with satellite retrieval accuracy. Meanwhile, during spring (MAM), both RPE and MBE exhibit an increasing trend and peak in April. This phenomenon is likely associated with rising temperatures and increased atmospheric water vapor content in spring, as water vapor absorption and scattering can disrupt satellite signals and amplify retrieval errors. In addition, spring also coincides with the peak biomass-burning season in Southeast Asia, during which aerosol optical depths over Guangxi can increase significantly due to transboundary transport[27,28]. The combined effect of elevated water vapor and higher aerosol loading—both of which attenuate surface solar radiation in ways not captured by the retrieval algorithm—likely contributes to the pronounced overestimation observed in spring.

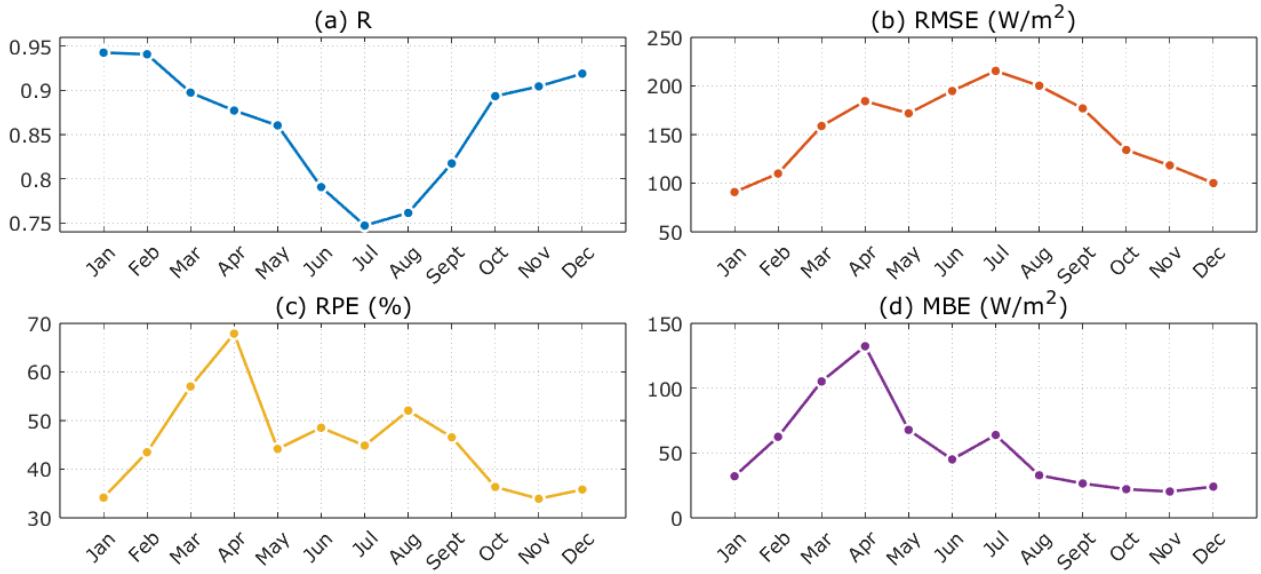

Figure 4. Monthly variations of R, RMSE, RPE, and MBE in 2023.

One major advantage of geostationary satellites is their ability to continuously monitor a fixed region at high temporal resolution. Accordingly, **Figure 5** presents hourly scatterplots comparing ground observations and Himawari-9 DSSR retrievals. Overall, during the morning hours (08:00–11:00 local time), R consistently exceeds 0.8, indicating robust agreement and relatively high satellite data quality. After 12:00, R gradually decreases and drops to 0.63 by 17:00, reflecting a notable degradation in retrieval accuracy during the afternoon. This decline is mainly attributed to the development and intensification of convective clouds around midday, which increases uncertainties in cloud parameter retrieval and consequently affects DSSR estimates[29]. The RPE remains relatively stable at approximately 40% between 09:00 and 13:00, suggesting comparatively smaller relative errors during this period. In contrast, RPE increases significantly during early morning (07:00–08:00) and late afternoon (16:00–17:00), reaching its maximum at 17:00, indicating the largest retrieval errors. This degradation during sunrise and sunset periods is primarily related to low solar elevation

angles. At very low sun angles, atmospheric path length increases substantially, amplifying uncertainties in atmospheric parameter retrieval and leading to larger errors in DSSR estimation [30,31]. Meanwhile, the plane-parallel atmospheric assumption adopted in DSSR retrieval algorithms neglects atmospheric curvature and refraction effects, which is valid for high solar elevations but becomes increasingly inaccurate under low solar angles, leading to distorted estimates near sunrise and sunset. The diurnal variation of RMSE generally follows that of surface solar radiation intensity. The diurnal pattern of MBE indicates that satellite overestimation is more pronounced in the morning than in the afternoon, with the maximum overestimation occurring around local noon (12:00–13:00).

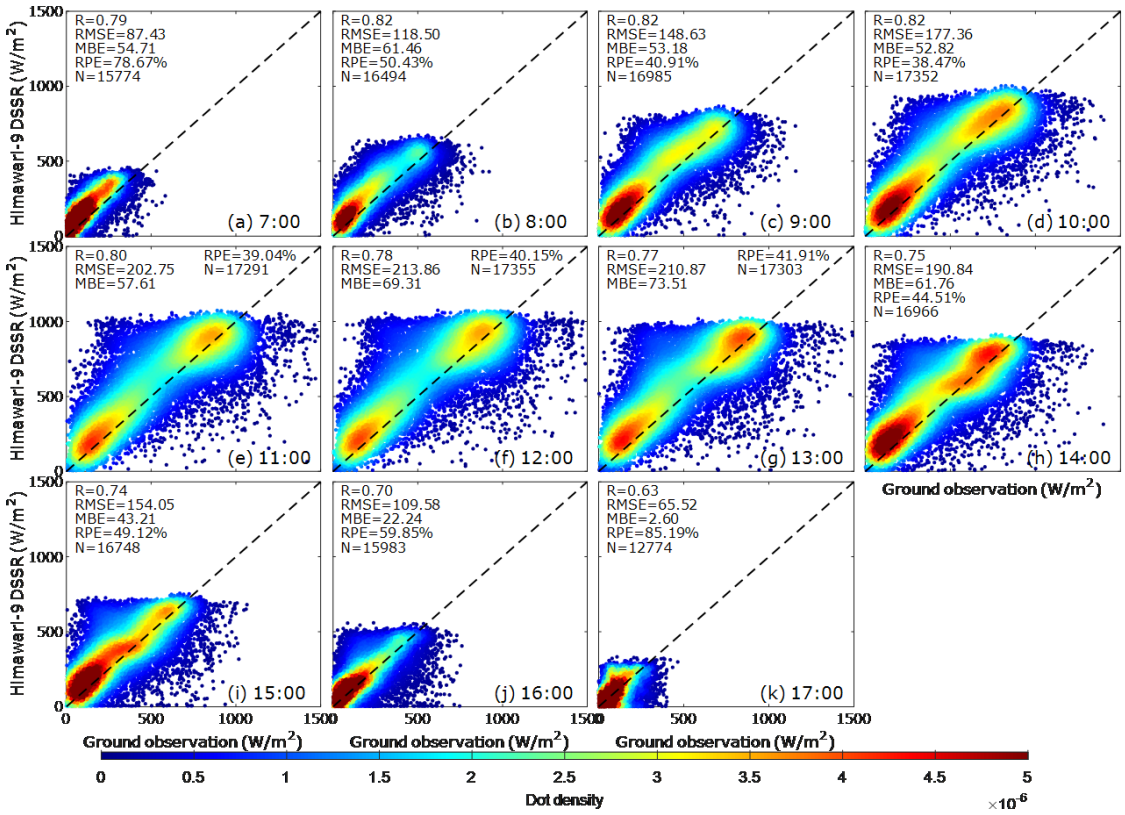

Figure 5. Hourly scatterplots of DSSR between Himawari-9 satellite retrievals (vertical axis) and ground station observations (horizontal axis) in 2023.

Statistical metrics (R, RMSE, RPE, and MBE) are further calculated for each ground station to derive their spatial distributions (**Figure 6**) and city-level aggregated results (**Table 1**). Overall, correlation coefficients across Guangxi mainly range from 0.75 to 0.90 (**Figure 6a**), with 91% of stations exhibiting R values in excess of 0.8, indicating a robust linear consistency between the satellite retrievals and ground observations. However, other error metrics reveal pronounced spatial heterogeneity. As shown in **Table 1**, RMSE values are generally high, with 9 out of 14 cities (64%) exceeding 150 W/m^2. The most significant RMSE values are observed in Yulin (178.31 W/m^2), Laibin (168.23 W/m^2), and Beihai (166.14 W/m^2). City-level RPE ranges from 41.66% in Chongzuo to 60.64% in Hechi. Geographically, southern and central cities such as Chongzuo, Beihai, and Qinzhou exhibit RPE values below 45%, whereas western and northern cities, including Hechi and Liuzhou, show substantially higher RPE. Notably, MBE is positive for all cities, confirming a systematic overestimation of DSSR by the Himawari-9 product across Guangxi. The most severe overestimations occur in Hechi (96.39 W/m^2), Liuzhou (87.24 W/m^2), and Laibin (70.80 W/m^2). Considering the regional geographical context, areas with larger errors are mainly concentrated in northern and western Guangxi, where mountainous and hilly terrain, frequent cloud cover, and complex atmospheric conditions prevail. In contrast, stations with relatively smaller

errors are mostly located in southern and central Guangxi (e.g., Chongzuo, Beihai, and Nanning), characterized by flatter terrain and higher atmospheric transparency. This spatial pattern suggests that terrain complexity likely influences retrieval accuracy through multiple mechanisms. Complex topography can promote orographic cloud formation, leading to more persistent cloud cover that challenges the satellite algorithm. Additionally, variable surface elevation within a satellite pixel (5 km resolution) introduces representativeness errors, as the retrieved DSSR represents a spatial average that may not correspond to the specific ground station location, particularly in regions with steep terrain gradients. Furthermore, mountainous areas may experience altered atmospheric path lengths and viewing geometries that deviate from the flat-surface assumptions in the retrieval algorithm. However, a rigorous quantitative assessment of these terrain effects is constrained by the relatively coarse 5 km spatial resolution of the Himawari-9 product, which cannot adequately resolve fine-scale topographic features across Guangxi's heterogeneous landscape. Future studies incorporating high-resolution digital elevation models and terrain complexity indices (e.g., elevation standard deviation, surface roughness) will be necessary to systematically quantify the relationship between topographic variability and DSSR retrieval errors, particularly as higher-resolution geostationary satellite products become available.

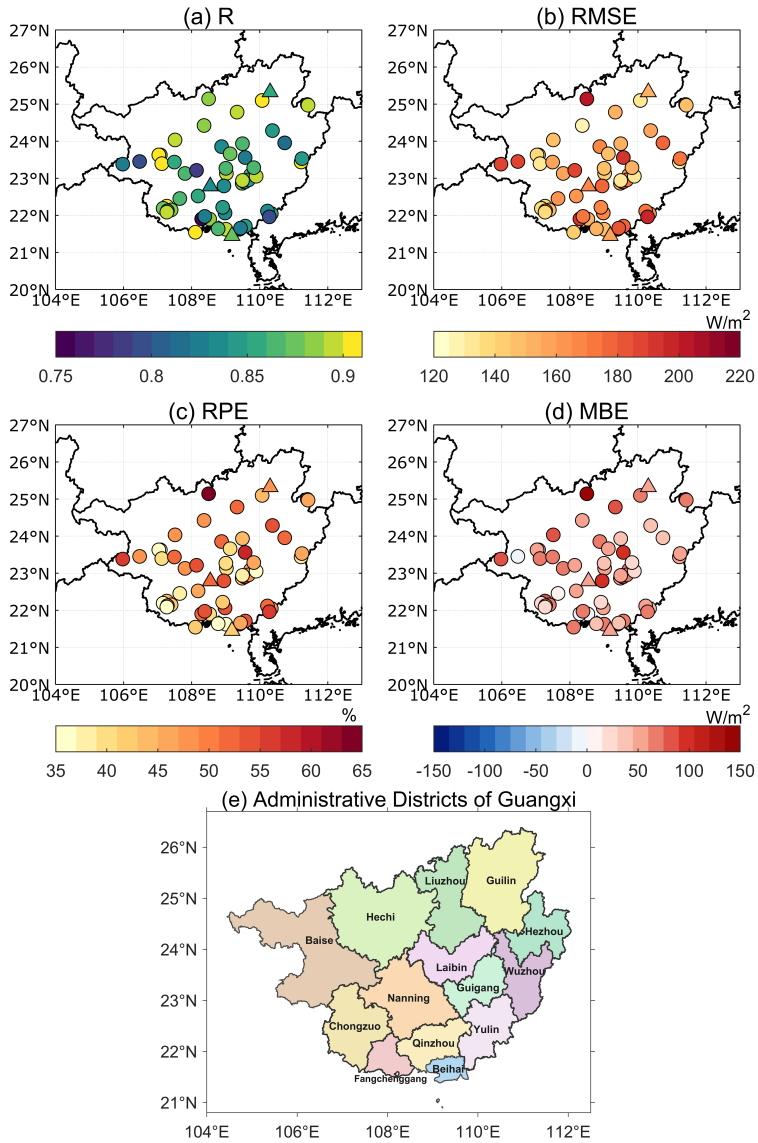

Figure 6. (**a**)–(**d**) are the spatial distribution of statistical metrics R, RMSE, RPE, and MBE, respectively. (**e**) shows the administrative districts of Guangxi.

Note: Circles denote photovoltaic stations, and triangles denote CMA stations.

Table 1. R, RMSE, RPE, MBE, and sample size (N) for 14 cities in Guangxi.

	R	RMSE (W/m^2)	RPE	MBE (W/m^2)	N
Nanning	0.85	162.08	47.69%	58.35	21,521
Liuzhou	0.90	151.35	52.25%	87.24	5,742
Guilin	0.88	144.31	45.56%	59.84	7,566
Wuzhou	0.85	157.16	47.60%	49.84	11,368
Beihai	0.86	166.14	44.28%	53.67	13,347
Fangchenggang	0.83	167.11	46.78%	28.99	6,362
Qinzhou	0.85	162.05	44.81%	33.08	16,288
Guigang	0.87	156.94	45.06%	53.38	17,920
Yulin	0.83	178.31	51.83%	55.81	9,893
Baise	0.86	157.85	44.76%	51.24	20,246
Hezhou	0.89	144.05	44.43%	60.67	7,228
Hechi	0.89	158.25	60.64%	96.39	7,167
Laibin	0.85	168.23	50.37%	70.80	10,050
Chongzuo	0.88	149.41	41.66%	42.90	22,682

Note: All reported R and MBE are statistically significant at the $p < 0.001$ level, given the large number of matched samples (N) for each city.

3.2. Effects of Clouds and Aerosols on the Quality of the Himawari-9 DSSR Product

The influence of cloud on the quality of the Himawari-9 DSSR product is further investigated. Cloud amount is quantitatively characterized using cloud optical depth (COD), with larger COD values indicating optically thicker cloud layers, and stronger absorption and scattering of solar radiation. Matched samples are divided into six COD intervals, and DSSR scatterplots were generated for each interval (**Figure 7**). Compared with all-sky conditions (**Figure 3a**), satellite retrievals under clear-sky conditions (**Figure 7a**) show much closer agreement with ground observations, with an R value of 0.90 and RMSE, RPE, and MBE values of 145.71 W/m^2, 38.43%, and 57.67 W/m^2, respectively. This indicates relatively high consistency between satellite and ground data under clear skies, although systematic overestimation persists. As COD increases, discrepancies between satellite retrievals and ground observations become progressively more pronounced, and overall product quality deteriorates. When COD exceeds 50 (**Figure 7f**), R decreases sharply to 0.11 and RPE increases to 122.54%, indicating that the Himawari-9 product is unable to reliably estimate DSSR under heavily overcast conditions. This near-zero correlation can be attributed to the saturation of the cloud retrieval algorithm under optically very thick conditions. When COD exceeds 50, both the $(1-A)$ term in the numerator and the $(1-S_aA)^{-1}$ term in the denominator of Equation (1) become highly sensitive to small errors in retrieved cloud albedo A, yet the algorithm's ability to distinguish further increases in COD is fundamentally limited. Consequently, the satellite produces systematically low and relatively uniform DSSR estimates, failing to capture the variability in actual surface-reaching radiation that arises from diffuse transmission through thick clouds. This behavior is consistent with known limitations of plane-parallel radiative transfer models under deep convective or multi-layer cloud systems, where three-dimensional radiative effects and photon trapping within clouds dominate[32]. Notably, under thin or partly cloudy conditions (e.g., COD ≤ 5; **Figure 7a–c**), MBE values remain large and positive, indicating substantial overestimation of DSSR. This likely arises from the limited sensitivity of the current retrieval algorithm to optically thin clouds[32], which fails to fully capture their subtle scattering and absorption effects. As cloud cover increases, the overestimation gradually weakens and eventually transitions to underestimation. For instance, when COD > 50 (**Figure 7f**), MBE becomes negative, reflecting an overemphasis of cloud attenuation in the retrieval algorithm. This behavior can be attributed to the simplified single-layer, isotropic cloud assumption, which cannot realistically represent complex multiple scattering processes within clouds. Furthermore, RMSE exhibits a non-monotonic response to increasing COD, initially increasing and then decreasing, with a peak in the moderate COD range ($1 < \text{COD} \leq 5$). Under thick cloud conditions, the absolute surface radiation itself is substantially reduced, leading to smaller absolute errors despite very large relative errors (e.g., RPE).

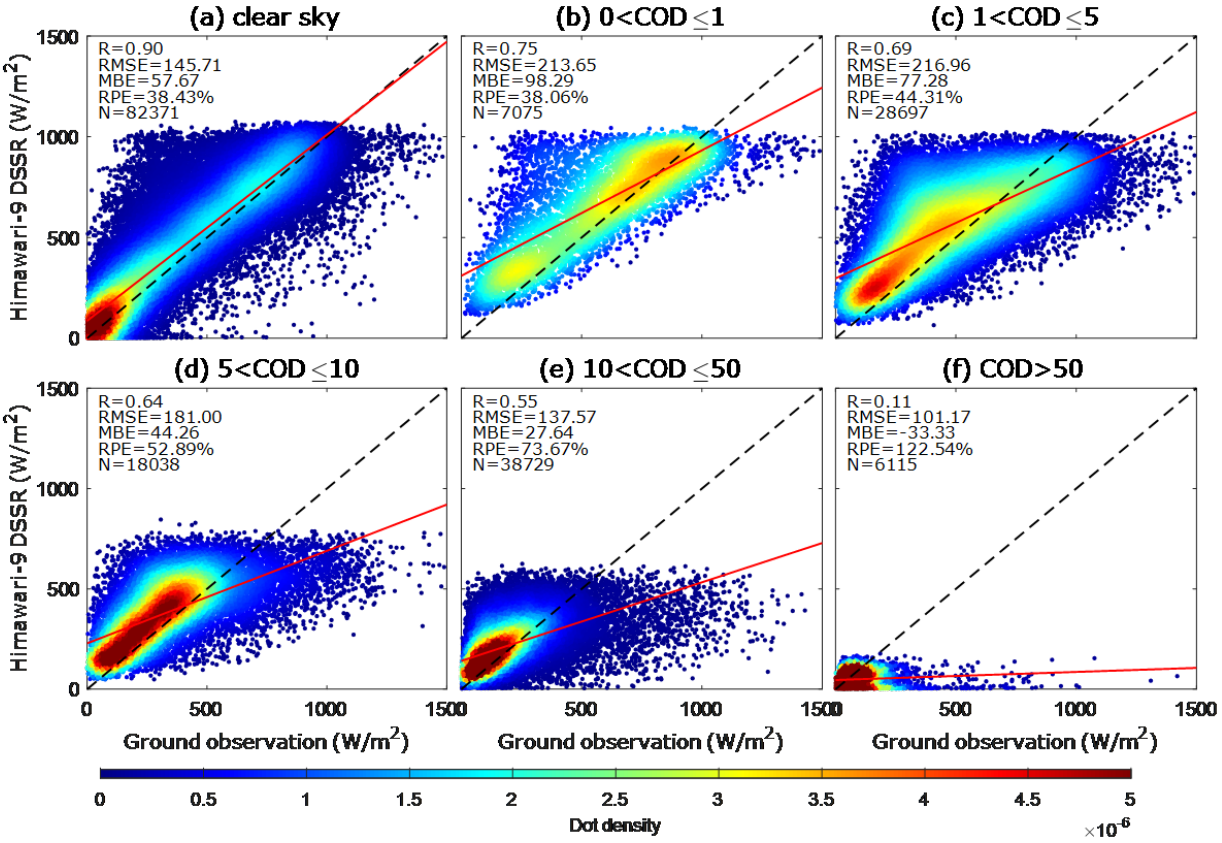

Figure 7. DSSR scatterplots under different cloud optical depth (COD) conditions.

The impact of aerosols on the Himawari-9 DSSR product is also examined. Aerosol loading is characterized by aerosol optical depth (AOD), defined as the column-integrated extinction coefficient of aerosols. Larger AOD values signify elevated aerosol concentrations, leading to enhanced extinction of incident solar radiation through combined scattering and absorption processes. Since AOD can only be reliably retrieved under clear-sky conditions, clear-sky matched samples were divided into six AOD intervals, and corresponding DSSR scatterplots were generated (**Figure 8**). Consequently, the sample size in **Figure 8** is smaller than that in **Figure 7**. Our results indicate that, relative to the dominant influence of clouds, aerosols exert a more moderate yet statistically significant effect on DSSR retrieval fidelity. The correlation coefficient R decreases slightly from 0.84 to 0.79 as AOD increases. However, other error metrics exhibit pronounced degradation: RMSE increases from 128.75 W/m^2 to 229.84 W/m^2, MBE increases from 46.46 W/m^2 to 164.39 W/m^2, and RPE rises from 19.99% to 49.40%. These results indicate that DSSR overestimation by the satellite becomes substantially more severe under high aerosol loading. The primary reason for this behavior is that the current retrieval algorithm does not explicitly account for aerosol radiative effects under clear-sky conditions and implicitly assumes a clean atmosphere. As aerosol concentrations increase, the actual surface-reaching radiation is increasingly attenuated, while the satellite continues to retrieve DSSR under aerosol-free assumptions, leading to systematic overestimation. Therefore, although the existing algorithm performs reasonably well under low-AOD conditions, it exhibits clear limitations in heavily polluted or dust-laden environments. Accurately representing aerosol radiative effects under clear skies remains a key challenge and an important direction for future improvements in geostationary satellite DSSR retrieval algorithms.

It should be noted that the spatiotemporal matching scheme (±1 h, nearest 5 km grid point) may introduce representativeness errors, particularly under rapidly evolving cloud and aerosol conditions. The temporal mismatch could lead to comparisons between satellite pixels and ground observations under substantially different atmospheric states, especially during the passage of convective

systems. Similarly, within a 5 km grid cell, significant subgrid spatial variability in cloud cover may exist, particularly in complex terrain. These factors contribute to the overall uncertainty in the statistical evaluation and should be considered when interpreting the results. Future work will explore the use of higher-resolution cloud and aerosol satellite products to reduce these spatiotemporal matching uncertainties.

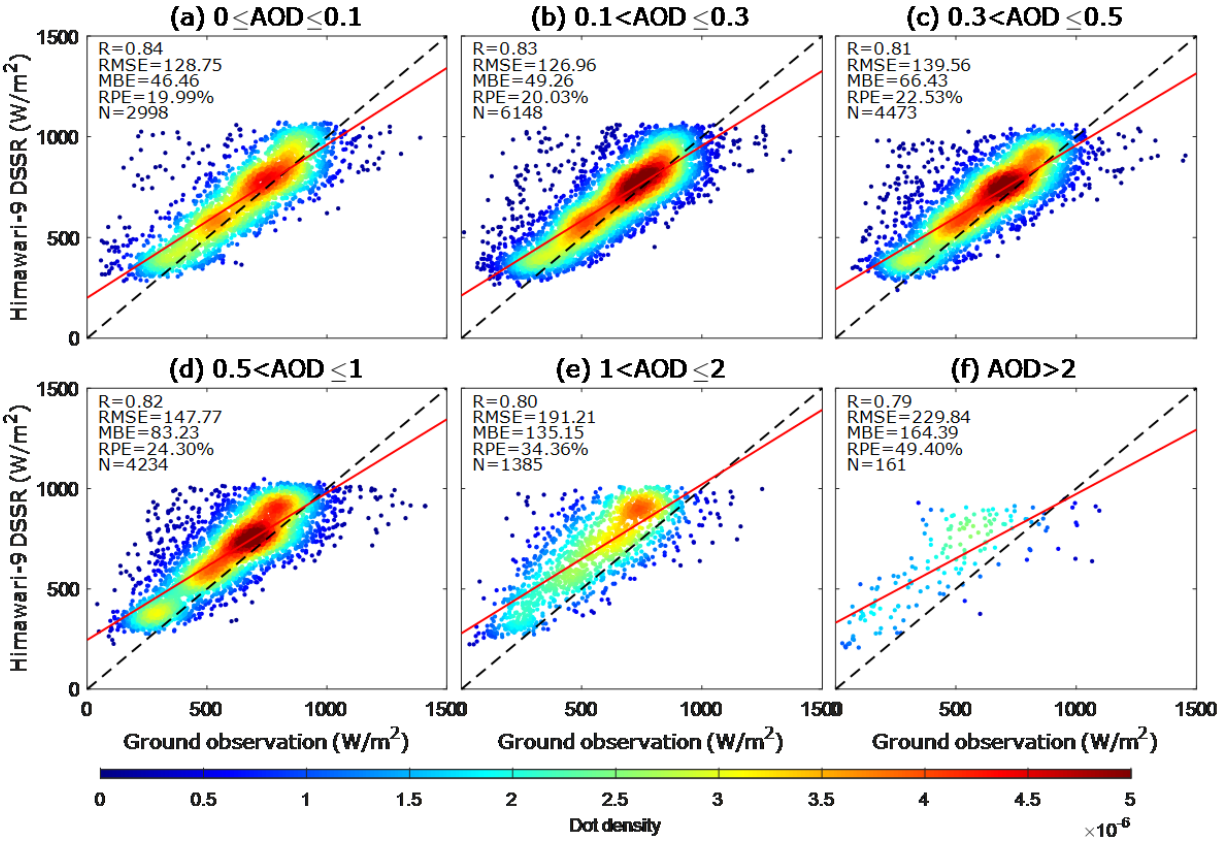

Figure 8. DSSR scatterplots under different aerosol optical depth (AOD) conditions.

4. Conclusions and Outlook

Based on surface solar radiation observations from 55 densely distributed PV stations and three national benchmark stations operated by CMA in Guangxi for the year 2023, this study conducts a systematic evaluation of the Himawari-9 satellite–retrieved DSSR product. Through rigorous quality control following BSRN recommendations, spatiotemporal matching, and multidimensional statistical analyses—including the correlation coefficient (R), root mean square error (RMSE), relative prediction error (RPE), and mean bias error (MBE)—the following main conclusions are drawn.

1) Overall performance is satisfactory, but systematic biases persist. The Himawari-9 DSSR product exhibits a strong linear relationship with ground-based observations (R = 0.85), indicating reasonable regional applicability. However, the RMSE reaches 162.99 W/m^2, the RPE is as high as 46.71%, and the MBE equals 51.53 W/m^2, demonstrating a pronounced systematic overestimation of surface shortwave radiation across Guangxi, with both absolute and relative errors remaining substantial.

2) Satellite retrieval errors exhibit pronounced spatiotemporal heterogeneity. On a seasonal scale, the largest errors occur in spring (MAM) and summer (JJA). Spring shows the highest MBE (100.45 W·m^{-2}) and RPE (54.40%) of the year, while summer exhibits the largest RMSE (203.78 W·m^{-2}) and the lowest correlation (R = 0.77), largely influenced by the seasonal evolution of precipitation and cloudiness. On a diurnal scale, satellite retrievals perform best during the morning hours (08:00–11:00 local time; R > 0.8), whereas er-

rors increase significantly during early morning and late afternoon, which is closely associated with the breakdown of the plane-parallel atmospheric assumption under low solar elevation angles. Spatially, better performance is observed in southern and central Guangxi (e.g., Chongzuo and Beihai), characterized by relatively flat terrain, while larger errors are found in mountainous northwestern cities such as Hechi and Liuzhou. This spatial pattern highlights the challenges posed by complex terrain for modeling clouds, aerosols, and radiative transfer processes.

3) Clouds and aerosols are key drivers of retrieval uncertainty, with clouds exerting a dominant influence. Satellite retrieval accuracy deteriorates rapidly with increasing COD. Under heavily overcast conditions (COD > 50), the correlation coefficient drops to 0.11, and the RPE increases to 122.54%. Moreover, the bias transitions from overestimation under thin-cloud conditions to underestimation under thick-cloud conditions, revealing deficiencies in the cloud assumptions employed by the retrieval algorithm. Although the impact of AOD is comparatively weaker, it remains non-negligible. Under clear-sky conditions with high AOD (>2), the MBE increases to 164.39 $W \cdot m^{-2}$, and the RPE reaches 49.40%, indicating significant overestimation caused by the neglect of aerosol radiative effects in the retrieval algorithm.

The overall performance of the Himawari-9 DSSR product over Guangxi (R = 0.85, RMSE = 162.99 W/m^2, MBE = 51.53 W/m^2, RPE = 46.71%) exhibits relatively higher errors than previously reported Himawari-8/9 evaluations in other regions. For instance, Yu et al. (2019)[16] reported a higher correlation ($R \approx 0.94$) and a moderate systematic overestimation across East Asia, while Damiani et al. (2018)[19] and Xu and Mao (2024)[18] found superior accuracy (R > 0.90) over Japan and Beijing, respectively, with both studies also observing systematic overestimation. In contrast, our results indicate that DSSR errors in Guangxi are notably higher than those reported for Japan and northern China (R = 0.85 vs. R > 0.90). This discrepancy can be attributed to the distinct climatic and geographical characteristics of southern China: Guangxi experiences more persistent cloud cover throughout the year, higher atmospheric humidity due to its subtropical monsoon climate, and more complex topography ranging from coastal plains to mountainous regions. These findings suggest that satellite product performance benchmarks established in relatively cloud-free and topographically simple regions (e.g., Japan, northern China) may not be directly transferable to humid subtropical environments with heterogeneous terrain. Regional adaptation and bias correction strategies tailored to local atmospheric and surface conditions are therefore necessary to improve DSSR retrieval accuracy in such complex environments.

In summary, this study represents the first comprehensive evaluation of the Himawari-9 DSSR product over a humid, cloud-prone, and topographically complex region of southern China using a high-density PV station observation network. The results reveal key limitations of the current retrieval algorithm, including insufficient sensitivity to thin clouds, excessive attenuation under thick clouds, and the omission of aerosol radiative effects under clear-sky conditions. These findings provide critical insights for improving geostationary satellite surface radiation retrieval algorithms. Importantly, the ground-truth dataset constructed from 55 distributed PV stations and three CMA national stations effectively overcomes the limitations of sparse conventional meteorological networks and poor spatial representativeness. This framework offers a replicable validation paradigm for other subtropical hilly regions facing similar challenges in terrain complexity and urgent energy transition needs. Beyond advancing the understanding of regional solar radiation spatiotemporal variability, this study establishes a robust data foundation for photovoltaic resource assessment, power plant site optimization, and power generation forecasting.

In addition to Himawari-8/9, China's domestically developed Fengyun-4 (FY-4) series geostationary satellites provide comparable or even higher spatiotemporal resolution and are better adapted to regional atmospheric and surface characteristics, offering substantial potential for solar energy resource monitoring. Future work will focus on multi-source geostationary satellite integration (e.g., FY-4 and Himawari-9) to develop fused radiation products, thereby improving the accuracy and reliability of surface solar radiation estimates over complex underlying surfaces in southern China and across the country. However, it is worth noting that FY-4 and Himawari-9 employ different retrieval algorithms and have distinct sensor characteristics, which may introduce systematic inter-satellite biases in fused products. Addressing these

challenges will require careful cross-calibration, harmonized cloud and aerosol parameterization, and region-specific bias correction. Beyond satellite data fusion, several methodological advances warrant investigation. First, machine learning-based post-processing techniques, such as random forests or deep neural networks trained on historical ground observations, show promise for correcting systematic biases and capturing nonlinear relationships between retrieval errors and environmental predictors. Second, assimilation of real-time ground measurements from expanding PV station networks into satellite retrievals could enable dynamic bias correction at sub-regional scales. Third, integration of numerical weather prediction model outputs—particularly high-resolution cloud-resolving simulations—may help constrain retrieval uncertainties during rapidly evolving weather conditions. Finally, as China's PV installed capacity continues to grow exponentially, the operational radiation monitoring network will become increasingly dense, providing unprecedented opportunities for validating and improving satellite products across diverse climatic and topographic regimes. These synergistic developments will collectively enhance the scientific foundation for China's renewable energy transition. Such advancements will provide more reliable data support for photovoltaic power planning, power output forecasting, and energy–meteorological services.

Author Contributions

Writing original draft, validation, software, methodology, Y.Q.; writing original draft, investigation, formal analysis, J.H.; writing original draft, supervision, project administration, funding acquisition, L.Z.; supervision, data curation, conceptualization, K.H.; validation, investigation, H.Z.; validation, data curation, J.T. All authors have read and agreed to the published version of the manuscript.

Funding

This study was funded by the key scientific and technological project of Guangxi Power Grid Company, “Research on Correction of Key Meteorological Factors of Photovoltaic Power Generation Based on Satellite Monitoring Data and Prediction Technology of Solar Irradiance” (GXKJXM20230261).

Institutional Review Board Statement

Not applicable.

Informed Consent Statement

Not applicable.

Data Availability Statement

Observations from photovoltaic (PV) power stations are subject to data confidentiality agreements and are therefore not publicly available. The Himawari-9 satellite products are publicly available from the Japan Aerospace Exploration Agency (JAXA) at http://www.eorc.jaxa.jp/ptree/index.html. Surface solar radiation observations from the China Meteorological Administration (CMA) national stations can be obtained from the official CMA website (http://www.cma.gov.cn/).

Acknowledgments

We sincerely thank the Meteorological Satellite Center (MSC) of the Japan Meteorological Agency (JMA) for making the Himawari-9 AHI data available. We also acknowledge the China Meteorological Administration (CMA) for providing surface solar radiation observations from national benchmark stations, and the photovoltaic (PV) power stations for contributing in situ radiation measurements used in this study.

Conflicts of Interest

The authors declare no conflict of interest.

References

[1] Trenberth KE, Fasullo JT, Kiehl J. Earth’s global energy budget. Bulletin of the American Meteorological Society. 2009; 90(3): 311–324.

[2] Stephens GL, Li J, Wild M, et al. An update on Earth’s energy balance in light of the latest global observations. Nature Geoscience. 2012; 5(10): 691–696.

[3] Wild M. Enlightening global dimming and brightening. Bulletin of the American Meteorological Society. 2012; 93(1): 27–37.

[4] Wild M, Folini D, Schär C, et al. The global energy balance from a surface perspective. Climate Dynamics. 2013; 40(11): 3107–3134.

[5] Yin J, Molini A, Porporato A. Impacts of solar intermittency on future photovoltaic reliability. Nature Communications. 2020; 11(1): 4781.
[6] Jin H, Wang SJ, Yan P, et al. Spatial and temporal characteristics of surface solar radiation in China and its influencing factors. Frontiers in Environmental Science. 2022; 10: 973050.
[7] Hakuba MZ, Folini D, Sanchez-Lorenzo A, et al. Spatial representativeness of ground-based solar radiation measurements. Journal of Geophysical Research: Atmospheres. 2013; 118(15): 8585–8597.
[8] Huang G, Li Z, Li X, et al. Estimating surface solar irradiance from satellites: Past, present, and future perspectives. Remote Sensing of Environment. 2019; 233: 111371.
[9] Shi H, Li W, Fan X, et al. First assessment of surface solar irradiance derived from Himawari-8 across China. Solar Energy. 2018; 174: 164–170.
[10] Tang W, He J, Qi J, et al. A dense station-based, long-term and high-accuracy dataset of daily surface solar radiation in China. Earth System Science Data. 2023; 15(10): 4537–4551.
[11] Liang S, Wang D, He T, et al. Remote sensing of Earth's energy budget: Synthesis and review. International Journal of Digital Earth. 2019; 12(7): 737–780.
[12] Xia XA, Yang D, Shen Y. Fengyun radiation services for solar energy meteorology: Status and perspective. Advances in Atmospheric Sciences. 2024; 42: 252–260.
[13] Li R, Wang D, Liang S. Comprehensive assessment of five global daily downward shortwave radiation satellite products. Science of Remote Sensing. 2021; 4: 100028.
[14] Yu YC, Shi J, Wang T, et al. All-sky total and direct surface shortwave downward radiation (SWDR) estimation from satellite: Applications to MODIS and Himawari-8. International Journal of Applied Earth Observation and Geoinformation. 2021; 102: 102380.
[15] Huang C, Shi H, Yang D, et al. Retrieval of sub-kilometer resolution solar irradiance from Fengyun-4A satellite using a region-adapted Heliosat-2 method. Solar Energy. 2023; 264: 112038.
[16] Yu Y, Shi J, Wang T, et al. Evaluation of the Himawari-8 shortwave downward radiation (SWDR) product and its comparison with the CERES-SYN, MERRA-2, and ERA-Interim datasets. IEEE Journal of Selected Topics in Applied Earth Observations and Remote Sensing. 2021; 12(2): 519–532.
[17] Lu L, Li Y, Liang L, et al. Diurnal variation in surface incident solar radiation retrieved by CERES and Himawari-8. Remote Sensing. 2024; 16(14): 2670.
[18] Xu L, Mao Y. Evaluation of two satellite surface solar radiation products in the urban region in Beijing, China. Remote Sensing. 2024; 16(11): 2030.
[19] Damiani A, Irie H, Horio T, et al. Evaluation of Himawari-8 surface downwelling solar radiation by ground-based measurements. Atmospheric Measurement Techniques. 2018; 11(4): 2501–2521.
[20] Frouin R, Murakami H. Estimating photosynthetically available radiation at the ocean surface from ADEOS-II global imager data. Journal of Oceanography. 2007; 63(3): 493–503.
[21] Wang L, Lang Q, Wang Z, et al. Quantifying and mitigating errors in estimating downward surface shortwave radiation caused by cloud mask data. IEEE Transactions on Geoscience and Remote Sensing. 2024; 62: 1–15.
[22] He R, Zhou SY, Su Z, et al. Study on distribution characteristics and utilization suggestions of solar energy in Guangxi. Anhui Agricultural Science Bulletin. 2015; 21(24): 34–36. (in Chinese)
[23] Liang YL, Shen YB, Bai L, et al. Assessment of solar energy resource and its exploitation potential in South China. Journal of Applied Meteorological Science. 2017; 28(4): 481–492.
[24] Chen L, Liu C, Wang J, et al. How is the spatiotemporal representativeness of ground- and satellite-based aerosol optical depth (AOD) measurements over Asia?. Atmospheric Research. 2025; 315: 107857.
[25] Imai T, Yoshida R. Algorithm theoretical basis for Himawari-8 cloud mask product. Meteorological Satellite Center Technical Note. 2016; 61: 1–17.
[26] Khatri P, Iwabuchi H, Hayasaka T, et al. Retrieval of cloud properties from spectral zenith radiances observed by sky radiometers. Atmospheric Measurement Techniques. 2019; 12(11): 6037–6047.
[27] Huang X, Ding A, Liu L, et al. Effects of aerosol-radiation interaction on precipitation during biomass-burning season in East China. Atmospheric Chemistry and Physics. 2016; 16(15): 10063–10082.
[28] Chen J, Li C, Ristovski Z, et al. A review of biomass burning: Emissions and impacts on air quality, health and climate in China. Science of the Total Environment. 2017; 579: 1000–1034.
[29] Chepfer H, Brogniez H, Noel V. Diurnal variations of cloud and relative humidity profiles across the tropics. Scientific Reports. 2019; 9(1): 16045.
[30] Hu S, Gao TC, Li H, et al. Atmospheric polarization pattern simulation for small solar elevation angles and the analysis of atmospheric effect. Acta Physica Sinica. 2016; 65(1): 014203. (in Chinese)
[31] Herrería-Alonso S, Suárez-González A, Rodríguez-Pérez M, et al. A solar altitude angle model for efficient solar energy predictions. Sensors. 2020; 20(5): 1391.
[32] Huang Y, Siems S, Manton M, et al. Evaluating Himawari-8 cloud products using shipborne and CALIPSO observations: Cloud-top height and cloud-top temperature. Journal of Atmospheric and Oceanic Technology. 2019; 36(12): 2327–2347.